

# Magnetic order and electromagnon excitations in $\text{DyMnO}_3$ studied by neutron scattering experiments

T. Finger,<sup>1</sup> K. Binder,<sup>1</sup> Y. Sidis,<sup>2</sup> A. Maljuk,<sup>3,4</sup> D. N. Argyriou,<sup>3,\*</sup> and M. Braden<sup>1,†</sup>

<sup>1</sup>*II. Physikalisches Institut, Universität zu Köln, Zùlpicher Str. 77, D-50937 Köln, Germany*

<sup>2</sup>*Laboratoire Léon Brillouin, C.E.A./C.N.R.S., F-91191 Gif-sur-Yvette CEDEX, France*

<sup>3</sup>*Helmholtz-Zentrum Berlin, Hahn-Meitner Platz 1, D-14109 Berlin, Germany*

<sup>4</sup>*Leibniz Institute for Solid State and Materials Research Dresden, Helmholtzstrasse 20, 01069 Dresden, Germany*

(Dated: December 8, 2014)

Magnetic order and excitations in multiferroic  $\text{DyMnO}_3$  were studied by neutron scattering experiments using a single crystal prepared with enriched  $^{162}\text{Dy}$  isotope. The ordering of Mn moments exhibits pronounced hysteresis arising from the interplay between Mn and Dy magnetism which possesses a strong impact on the ferroelectric polarization. The magnon dispersion resembles that reported for  $\text{TbMnO}_3$ . We identify the excitations at the magnetic zone center and near the zone boundary in the  $b$  direction, which can possess electromagnon character. The lowest frequency of the zone-center magnons is in good agreement with a signal in a recent optical measurement so that this mode can be identified as the electromagnon coupled by the same Dzyaloshinski-Moriya interaction as the static multiferroic phase.

PACS numbers: 75.85.+t 75.30.Ds 75.47.Lx

## I. INTRODUCTION.

Strong magnetoelectric coupling may not only imply multiferroic order, i.e. a phase with coupled magnetic and ferroelectric order, but it can also result in hybridized collective excitations of combined polar phonon and magnetic character, which are called electromagnons<sup>1,2</sup>. Such excitations may interact with the electromagnetic radiation through the electric and the magnetic channels opening the path for multichroism effects<sup>3-5</sup>. The fact that these effects can be controlled through the multiferroic state might become of great technical relevance. By applying moderate electric fields multiferroic domains can be easily manipulated<sup>6-8</sup>, allowing one in consequence to switch the properties of reflected or transmitted electromagnetic radiation.

The understanding of the dynamic magnetoelectric effects, however, remains too limited. Following the discovery of the multiferroic phases in  $\text{REMnO}_3$ <sup>9-12</sup> with  $\text{RE}$  a rare earth, first evidence for electromagnon scattering was reported for this class of materials<sup>13</sup>. It seems intuitive to apply the same magnetoelectric coupling mechanism, which well explains the static multiferroic phases, to the collective excitations<sup>14</sup>. In many of the recently discovered transition-metal-oxide based multiferroics ferroelectric polarization,  $\vec{P}$ , can be explained with the model of inverse Dzyaloshinski-Moriya (DM) coupling<sup>15-17</sup> with:

$$\vec{P} \propto \vec{r}_{ij} \times (\vec{S}_i \times \vec{S}_j). \quad (1)$$

Here  $\vec{r}_{ij}$  is the distance vector between coupled spins  $\vec{S}_i$  and  $\vec{S}_j$ . The inverse DM coupling yields only weak

electromagnon scattering due to the small coupling coefficients arising from spin orbit coupling. Electromagnon scattering in  $\text{REMnO}_3$ , however, is quite strong and the main part of it cannot be modified by rotating the static cycloidal order<sup>18</sup>. While in  $\text{TbMnO}_3$  the multiferroic phase is characterized by a magnetic cycloid in the  $bc$  plane in zero magnetic field<sup>19-22</sup>, this plane flops to the  $ab$  plane<sup>23</sup> upon the application of magnetic fields along the  $a$  or the  $b$  direction as well as in the case of other RE's. In contrast the strong electromagnon response always appears for electric fields along the  $a$  direction<sup>18,24</sup>. A large variety of electromagnon measurements using optical or dielectric techniques were reported<sup>13,18,24-36</sup> as well as several theories to explain the strong electromagnon scattering along  $a$ <sup>18,37-41</sup>. In addition inelastic neutron scattering gives an insight to the magnetic character of these modes<sup>42-44</sup>.

Taking  $\text{TbMnO}_3$  as the prototypical material for the new class of multiferroics one may identify at least three electromagnon contributions in the optical and dielectric studies<sup>28,31,33</sup>: at 7.5 meV there is the strongest response followed by a signal at 2.7 meV (at 12 K). In addition there is a third electromagnon response at the low energy of 1.5 meV<sup>31</sup> that is more difficult to detect with optical methods due to its low energy and due to its small signal strength. For the contribution at the highest energy Valdés Aguilar et al.<sup>18</sup> presented a convincing explanation basing on a modulation of the symmetric exchange, that can be much stronger than that of the antisymmetric contributions. The structural distortion associated with the rotation of the  $\text{MnO}_6$ -octhedrons around the  $c$  axis generates strong coupling between a collective displacement of the planar oxygen ions against the Mn ions and a magnetic mode near the zone boundary of the magnetic zone<sup>18</sup>, see discussion below. It is widely accepted that this exchange-striction mechanism does explain the strong electromagnon response at

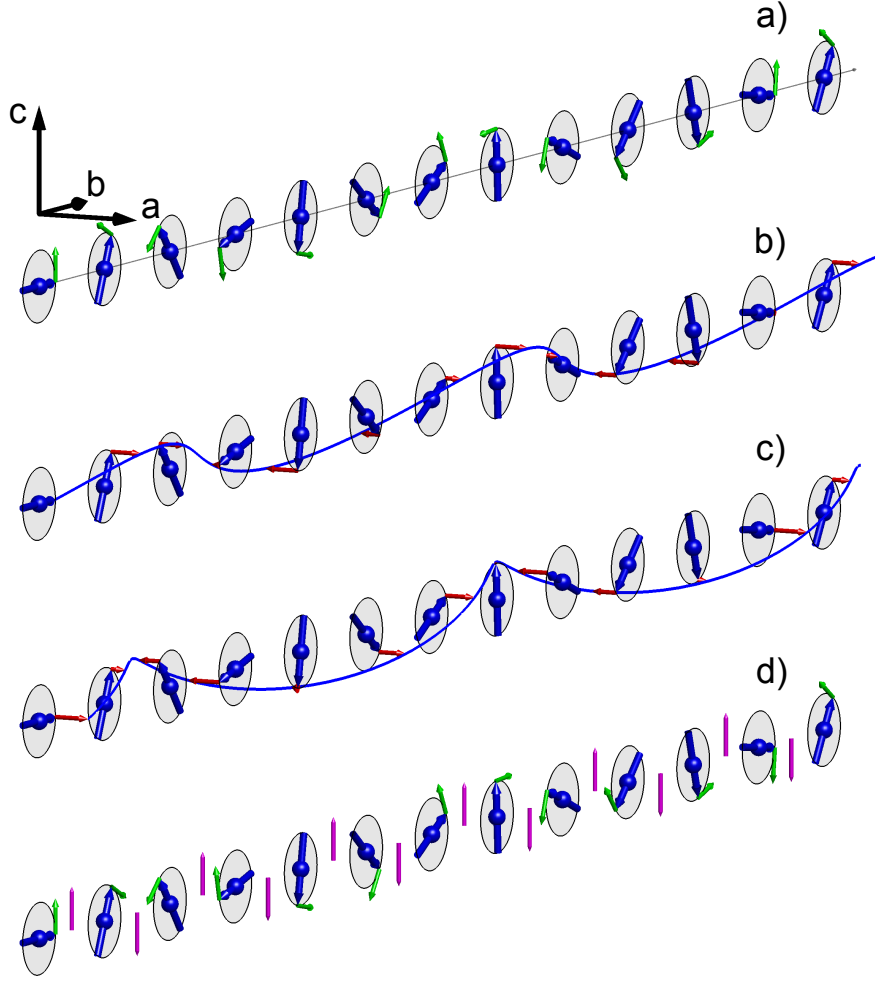


FIG. 1: (Color online) Illustration of polarization patterns of several magnon modes which are relevant for the discussion of electromagnons in  $\text{DyMnO}_3$ . In all parts the static cycloid is shown by large (blue) arrows rotating in the cycloid plane indicated by the shaded circles. The propagation vector of the modulation in  $b$  corresponds to that in  $\text{DyMnO}_3$  with two Mn per layer and unit cell. Part a) shows the pattern of the phason mode at the magnetic zone center. The frozen-in oscillating displacements of the spins are indicated by the small (green arrows). Adapting the inverse Dzyaloshinski-Moriya interaction described by equation (1) does not result in an oscillating polarization, because the cross product  $(\vec{S}_i \times \vec{S}_j)$  is constant. Part (b) shows the CRM associated with the rotation of the entire cycloid around the  $b$  direction. In this mode the spin cross product and thus the electric polarization rotate around  $b$  so that there is an oscillating polarization along  $a$  which can couple with electromagnetic radiation with  $\vec{E}$  parallel  $a$ . Part (c) shows the HM in which the spiral plane rotates around the  $c$  axis modifying the character of the spiral from a pure cycloid to a partial helical one. Applying equation (1) this will yield only a quadratic coupling with the electric polarization. Part (d) gives the polarization of the mode polarized within the cycloid plane ( $b, c$  plane) appearing at the propagation vector with  $k$  component  $k_{elm-str}=1-k_{inc}=0.64$ . This mode gains a strong oscillating electric polarization through the exchange striction mechanism. In the static cycloid the scalar product  $\vec{S}_i \cdot \vec{S}_j$  is constant; its momentous deviation from the average value is indicated by the vertical (magenta) bars.

high energy. In addition the static mechanism must also be relevant<sup>14</sup> and explains the electromagnon signal at the lowest energies<sup>13,31,33,35,36</sup>, which, however, possesses much lower spectral weight. The intermediate electromagnon, however, still needs further studies and a signal at even higher energies is most likely not related to an intrinsic electromagnon scattering<sup>28</sup>.

Comprehensive inelastic neutron scattering experiments in the cycloidal phases of  $\text{TbMnO}_3$  yield a microscopic characterization of the magnon excitations and strong support for the picture described above<sup>42-44,53</sup>. First the modes near the magnetic zone boundary in  $b$  direction indeed exhibit energies where the strongest electromagnon scattering is found in the optical studies. Three magnon modes can be identified at the magnetic

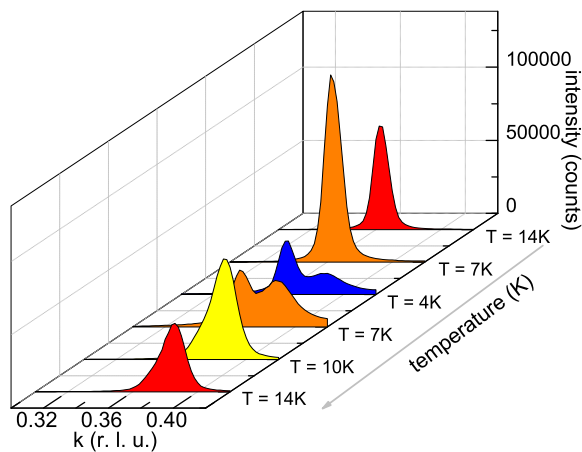


FIG. 2: (Color online) Temperature dependence of the magnetic (0  $k$  1) reflection measured from isotopically enriched DyMnO<sub>3</sub> single crystal. Data were collected on the 4F2 spectrometer upon cooling and heating (counting time  $\sim 60$ s), note the different peak position observed even far above the ordering temperature of Dy moments.

zone center, e.g. at  $\vec{Q} = (0 \ 0.28 \ 1)$  or  $\vec{Q} = (2 \ 0.28 \ 1)$ , and are illustrated in Fig. 1 a)-c). One mode can be associated with the oscillation of the phase of the cycloid, i.e. the phason. This mode cannot induce any electromagnon character, because the vector product of the neighboring spins and thus the induced polarization do not vary, see equation (1) and Fig. 1 a). Two other modes are characterized by the rotation of the cycloid plane around the  $b$  and the  $c$  direction, respectively<sup>14,42</sup>. Neglecting any anisotropies the mode for the rotation around the  $b$  direction, see Fig. 1 b), can be considered as the Goldstone mode of the multiferroic transition and should possess zero energy (being thus massless)<sup>43</sup>. Applying equation (1) this mode is associated with the rotation of the ferroelectric polarization around  $b$  which corresponds to an oscillation of the polarization in  $a$  direction. This mode thus exhibits electromagnon character<sup>14,42</sup> and can be measured with optical techniques for  $\vec{E}(\omega) \parallel \vec{a}$ . By analyzing the possible anisotropy energies Senff et al.<sup>43</sup> deduced that this rotational mode of the cycloid should be the zone center magnon with the lower but still finite energy, and indeed the few spectroscopic studies capable to examine the dielectric response at low enough energies do find excitations at the corresponding energies<sup>13,31,33,35,36</sup>. The other  $a$  polarized zone center magnon changes the character of the cycloid towards a partial helical character, see Fig. 1 c). In order to differentiate between these two modes we will label the first one cycloid rotation mode (CRM, see Fig. 1 b)) and the second helical mode (HM, see Fig. 1 c)). The CRM corresponds to the proposal in reference<sup>14</sup>. It appears tempting to compare the intermediate electromagnon scattering in TbMnO<sub>3</sub> with the HM as indeed the frequencies match well. However, the strength of the dielectric signal does not agree with

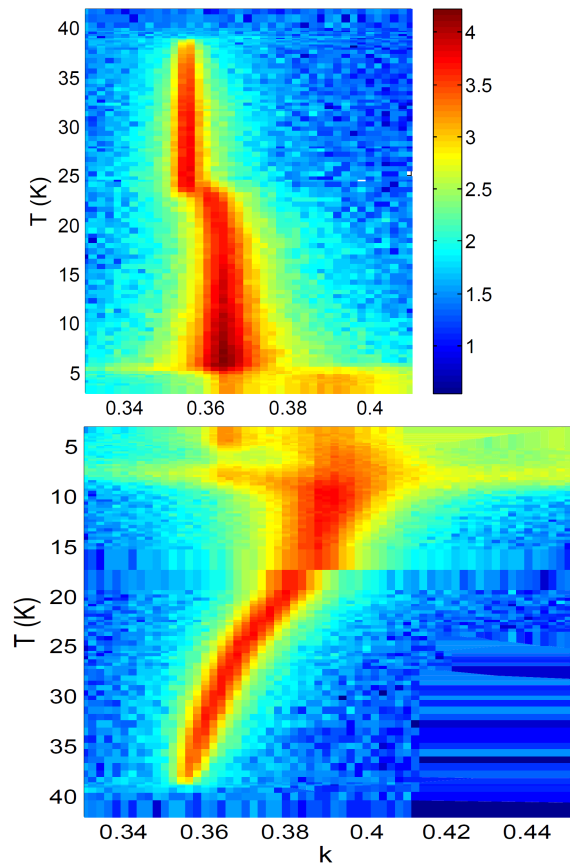


FIG. 3: (Color online) Temperature dependence of elastic magnetic scattering in DyMnO<sub>3</sub> at (0  $k$  1) studied on the 1T spectrometer upon cooling (above) and heating (below). At fixed temperatures the scattering intensity was recorded by scanning along (0  $k$  1). The color coding corresponds to a logarithmic scale for a counting time of about 15 s; note that the lower scans extend to larger  $k$  values.

the character of this mode. The electromagnon weight could arise through mixing with other modes<sup>18,38</sup> but it seems more likely that other magnon modes cause this intermediate electromagnon response through the more effective exchange striction mechanism<sup>38-40</sup>. Due to the flat dispersion between (0 0 1) and the magnetic Bragg point many magnon modes possess energies in this range.

While the electromagnon response in the various REMnO<sub>3</sub> compounds has been studied with different dielectric or optical techniques, so far only multiferroic TbMnO<sub>3</sub> has been studied by inelastic neutron scattering, because of the high neutron absorption of natural Sm, Eu, Gd and Dy. In this work we have used Dy with enriched <sup>162</sup>Dy isotope content to grow a large crystal that is suitable for inelastic experiments. The sequence of magnetic transitions in DyMnO<sub>3</sub> is similar to that in TbMnO<sub>3</sub><sup>19-22</sup>, with a first transition to a longitudinal

spin-density wave along  $b$  at 38 K followed by the development of cycloidal order in the  $bc$  plane at 18 K and the onset of ordering of Dy moments below 10 K<sup>45–47</sup>. However, the interplay between RE and Mn magnetism seems to be stronger in the Dy compound which is assumed to contribute to enhanced ferroelectric polarization<sup>46</sup>. Indeed we find pronounced hysteresis effects in the Dy as well as in the Mn ordering as function of temperature. The magnetic excitations and their dispersion also strongly resemble the findings in TbMnO<sub>3</sub>, which somehow contrasts with the different electromagnon response in DyMnO<sub>3</sub> reported by the dielectric studies.

## II. EXPERIMENTAL

A large single crystal of DyMnO<sub>3</sub> was grown by the travelling floating-zone technique in an image furnace. The feed rod was synthesized with a <sup>162</sup>Dy isotope content enriched to 90% while a seed crystal with natural Dy was used. The crystal was characterized by SQUID measurements which may identify the ordering of Dy moments at 5.4(3) and 7.1(3) K upon cooling and heating, respectively<sup>48</sup>. Measurements of specific heat allow one to determine three ordering temperatures by the maxima in  $c_p/T$  at 5.7(3), 18.8(3) and 38.2(3) K<sup>48</sup> in perfect agreement with previously reported measurements<sup>45–47</sup> and the neutron diffraction experiments described below.

Elastic and inelastic neutron scattering experiments were performed with the cold triple-axis spectrometer 4F2 ( $k_f=1.55 \text{ \AA}^{-1}$ ) and with the thermal triple-axis spectrometer 1T ( $k_f=2.66 \text{ \AA}^{-1}$ ) at the Orphée reactor in Saclay. At 4F2 a double monochromator and an analyzer using the (002) reflection of pyrolytic graphite (PG) were utilized, and a Be filter was set between the sample and the analyzer in order to suppress higher-order contaminations. On 1T a PG monochromator, a PG analyzer and a PG filter were used. Two cylindrical crystals of about 4 mm thickness and  $\sim 5$  mm diameter were coaligned into the [010]/[001] scattering geometry for the 4F2 experiment; for the structural studies on 1T a smaller single piece of the same growth was mounted. Throughout the paper we use reduced lattice units to address scattering vectors referring to the orthorhombic lattice in the setting of  $Pbnm$  with  $a=5.27$ ,  $b=5.83$  and  $c=7.35 \text{ \AA}$ . The sample was cooled with an orange-type liquid-helium cryostat and a closed-cycle refrigerator on 4F2 and 1T, respectively.

## III. RESULTS AND DISCUSSION

### A. Magnetic ordering in DyMnO<sub>3</sub>

The sequence of magnetic transitions in DyMnO<sub>3</sub> has been studied using resonant and non-resonant X-ray techniques<sup>45–47</sup>. These studies only give access to the

intrinsic ordering of Dy moments and to the structural distortions accompanying the ordering of Mn moments. In contrast, the ordering of Mn moments was not studied so far. Compared to TbMnO<sub>3</sub> the emergence of magnetic order is qualitatively similar but the Dy moments seem to possess a stronger impact even far above the onset of full order of these moments. Upon cooling, ordering of Mn moments sets in at  $T_N=38.2$  K with an incommensurate modulation along the  $b$  direction described by the propagation vector  $(0 \ 0.36 \ 0)$ . We study the magnetic ordering near  $\vec{Q}=(0 \ 0.36 \ 1)$  which takes into account the antiferromagnetic coupling along the  $c$  direction. The temperature dependence of the wavelength of the magnetic modulation was previously studied via the coupled lattice modulation of half the wave length corresponding to the doubled pitch of the propagation vector. Strempler et al. find a pronounced hysteresis between cooling and heating cycles<sup>47</sup>. With our neutron diffraction experiment we may directly analyze the ordering of the Mn moments and we can confirm the strong difference between cooling and heating cycles, see Fig. 2, which displays data obtained with the large sample on 4F2. In the first cooling from room temperature we find a peak centered near  $(0 \ 0.363 \ 1)$  which strongly increases in intensity upon cooling to 7 K. Upon further cooling below the onset of magnetic order of Dy moments, which corresponds to a different propagation vector of  $(0 \ 0.5 \ 0)$ , the signal of the Mn moments seems to split with an additional contribution appearing at  $(0 \ 0.39 \ 1)$ . Reheating to 7K, however, does not yield the initial peak but the additional contribution becomes enhanced and finally dominant at 10 K. Even heating to 14 K does not yield the initial arrangement although this temperature is well above the suppression of Dy moment order, which disappears upon heating at 7.1 K, as observed in the SQUID data. In order to further elucidate this complex hysteresis, two full cooling and heating cycles were recorded on the 1T spectrometer which yielded identical results, but only one cycle is shown in Fig. 3. The scans across the signals arising from the Mn moments were fitted by one or two Lorentzian peaks yielding the results resumed in Fig. 4.

Fig. 3 demonstrates the pronounced hysteresis of the Mn spin order between cooling and heating which can be perfectly explained by the coupling of the Dy and Mn magnetism and by a strong coupling of the anisotropic Dy ions with the lattice. Upon cooling we find the propagation vector near  $(0 \ 0.36 \ 1)$  and an onset of Bragg scattering at  $T_N=38.2$  K, see Fig. 4. Cooling till about 25 K results in little variation of the modulation but in a strong intensity increase, which however suddenly drops at further cooling accompanied with a step in the modulation vector. The second magnetic transition associated with the onset of ferroelectric order is visible as a kink in the temperature dependence of the magnetic modulation, see inset of Fig. 4 b), which stays constant at

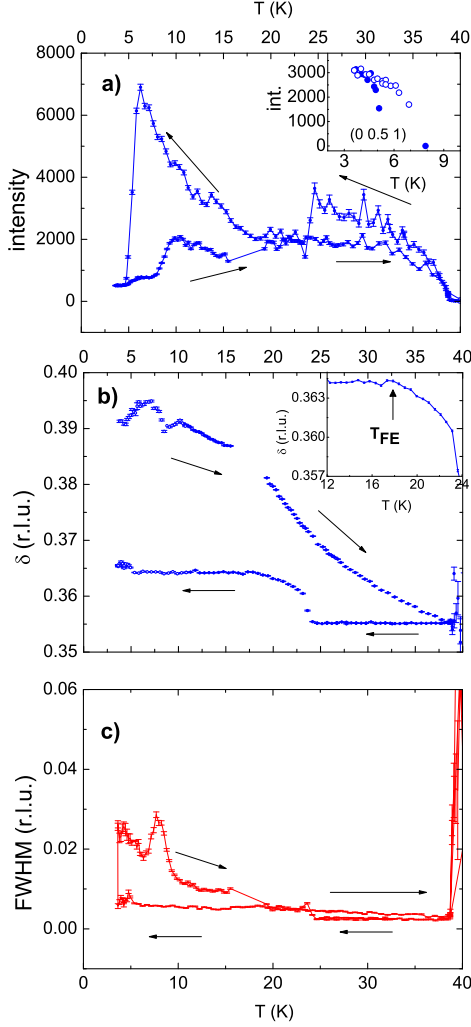


FIG. 4: (Color online) Temperature dependence of elastic magnetic  $(0\ k\ 1)$  scattering in  $\text{DyMnO}_3$  studied on the 1T spectrometer upon cooling and heating. The  $(0\ k\ 1)$  scans shown in Fig. 3 were fitted by one or two Lorentzian peak profiles (see Fig. 3). Panel a) shows the peak intensity (height) of the strongest peak as function of temperature, in addition the inset displays the height of the  $(0\ 0.5\ 1)$  peak that is associated with the ordering of Dy moments upon cooling and heating with closed and open symbols, respectively. Panel b) gives the incommensurate pitch (peak position) of the strongest signal; at low temperatures (open symbols) the measured profiles were fitted with two Lorentzians. The inset displays an enlargement of the temperature range near 18 K corresponding to the onset of ferroelectric order. Panel c) shows the temperature dependence of the full width at half maximum (FWHM) of the fitted peak profiles, which senses the impact of the Dy ordering.

lower temperatures. The intensity of the magnetic signal at  $(0\ 0.363\ 1)$  sharply increases upon further cooling indicating a stronger modulation of Dy moments with the same period as that of the Mn moments. This additional intensity is suppressed at the magnetic ordering of Dy moments near 5 K, see inset of Fig. 4a), because

Dy moments order at a distinct propagation vector of  $(0\ 0.5\ 0)$ . The onset of the Dy moment order is also visible in the broad diffuse scattering accompanying the transition that extends even beyond the wave vector of the Mn moments. Concomitantly, the Mn order becomes unpinned and exhibits a double signal. The additional Mn moment modulation appears at  $(0\ \sim 0.39\ 1)$ . This modulation seems to be responsible for the signal observed in resonant x-ray diffraction at the Dy edge near  $(0\ 2.9\ 3)$  which is just the combination of the intrinsic Dy order and the latter modulation of the Mn moments. The two values observed for the modulation of Mn moments most likely arise from strong and minor contribution of Dy moments to the two modulations, respectively. These results qualitatively agree with the modulations found at the doubled wave vectors with x-ray techniques<sup>45–47</sup>, but the isotope enriched crystal seems to exhibit slightly smaller incommensurabilities.

The lower part of Fig. 3 shows the following heating sequence. In the temperature range till 7 K there is some variation of the pitch of the additional Mn signal which becomes dominating upon heating. Again the loss of Dy order near 7.1 K, see inset of Fig. 4a), is visible in the broad intensity distribution. Above this transition, only the Mn signal at larger  $k$  remains and it exhibits a similar intensity compared to that of the initial signal upon first cooling indicating again a strong contribution of the Dy moments. But note that the modulation vector of the Mn order at 10 K is different for cooling and heating, which explains hysteretic effects in the ferroelectric polarization<sup>10</sup>.

The hysteresis of the Mn-moment magnetism in this broad temperature range is remarkable. It arises from two effects: the intrinsic hysteresis of the Dy order and the hysteresis of the coupling of Dy and Mn moments with differing preferred propagation vectors. The latter results in the two  $k$ -components of the propagation vectors of the Mn ordering of 0.36 and 0.39. Upon cooling the Dy order cannot induce the transformation of the Mn ordering to the larger values as it happens at too low temperature. Upon heating the Dy order shifts to 7.1 K and this extended temperature range seems sufficient to fully transform the Mn order to the larger  $k$ -component. In order to recover the initial scheme of Mn moment ordering one has to heat up to close to  $T_N$ . The modulation of the Mn order only smoothly decreases with heating towards the initial values due to the continuous depinning and due to the melting of Dy moments. Fig. 4c) shows the temperature dependence of the widths of the fitted peak profiles at  $(0\ \sim 0.4\ 1)$  arising from the ordering of Mn moments. Above  $T_N$  the magnetic scattering of course becomes very broad, but also near the onset and the disappearance of the Dy order the Mn magnetism is heavily perturbed. In addition the interplay seems to imply a finite width of the Mn signal in the almost entire temperature range, just upon the first cooling slightly below  $T_N$  sharp magnetic peaks exist.

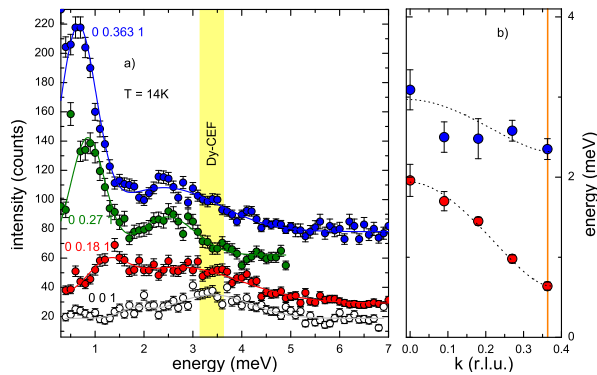


FIG. 5: (Color online) Panel a) shows constant  $\vec{Q}$  scans to determine the low-energy magnetic excitations between  $\vec{Q}=(0\ 0.363\ 1)$  and  $(0\ 0\ 1)$  and dispersion. Slightly above the energy of 3 meV some signal may arise from a Dy crystal field excitation of the lifting of Kramers doublet degeneracy. Panel b) shows the flat dispersion in this part of the Brillouin zone.

Resuming these elastic studies, we find a close coupling between the magnetism of Dy and Mn moments with very pronounced pinning effects. These hysteresis and pinning effects possess a clear impact on the ferroelectric polarization. The pyrocurrent measurements by Goto et al.<sup>10</sup> were taken upon heating; they show a huge difference between two runs recorded after cooling down to 2 and 7 K, respectively, which reflects the essential differences in the Mn ordering observed upon cooling and heating shown in Fig. 2 and 3. Apparently the longer wave-length magnetic modulation appearing upon cooling results in an up to  $\sim 50\%$  larger ferroelectric polarization. A strong hysteresis is also observed in the dielectric constant along  $c$  measured on a thin film of  $\text{DyMnO}_3$ <sup>49</sup>. In this dielectric measurement cooling and heating results fall together only above the Néel temperature, resembling our findings for the modulation vector of Mn moments.

## B. Magnetic excitations in $\text{DyMnO}_3$

Magnetic excitations were studied on the 4F2 spectrometer using cold neutrons,  $k=1.55\text{\AA}^{-1}$ . The main part of these measurements were performed at  $T=14\text{ K}$  in the multiferroic phase<sup>11,48</sup> but well above the ordering of Dy moments. Nevertheless Dy moments are already sizeably polarized at this temperature which implies a more complex magnon dispersion. Data were taken after cooling the sample to 10 K only. The crystal-field excitations in  $\text{DyMnO}_3$  were not yet studied by inelastic neutron scattering, and an infrared experiment detected only one crystal field excitation at 22.9 meV, which lies far above the energy range studied here<sup>50</sup>. Lower crystal field energies were just calculated to amount to 5.7 and 15.7

meV<sup>50</sup>. At the lower of these values we do not find evidence for a strong crystal field scattering. However, the same experiment reports a splitting of the Kramers doublet degeneracy by the interaction between Mn and Dy moments of 3.7 meV<sup>50</sup>, which might agree with a weak  $\vec{Q}$  independent signal in our scans, see Fig. 5, but for an unambiguous interpretation further studies are needed. The dispersive features discussed in the following cannot be attributed to Dy crystal-field excitations.

In view of the discussion of electromagnons, magnetic excitations at the zone center, i.e. taken at the magnetic Bragg points, are most important, as these modes may couple with infinite wavelength structural distortions even in the harmonic case. Data taken at  $\vec{Q}=(0\ 0.363\ 1)$  and other scattering vectors towards  $\vec{Q}=(0\ 0\ 1)$  are shown in Fig. 5. At the magnetic zone center one may recognize a low-energy mode at 0.8 meV and another one near 2.3 meV. At this scattering vector modes polarized in  $a$  direction fully contribute while a mode polarized in the  $c$  direction is strongly suppressed. Note that in general neutron scattering only senses the magnetic components polarized perpendicular to the scattering vector<sup>51</sup>. It appears thus reasonable to identify the two observed modes with the  $a$  polarized modes arising from the rotations of the cycloid planes<sup>42</sup>, CRM and HM, see Fig. 1 b) and c). Furthermore, the observed frequencies agree with those reported in  $\text{TbMnO}_3$  at slightly higher temperature: energy of HM at 2.5 meV and energy of CRM at 1.1 meV at  $T=17\text{ K}$  in  $\text{TbMnO}_3$ . Also the rather flat dispersion between the magnetic zone center and  $(0\ 0\ 1)$ , which can be discerned for at least two branches, resembles the behavior in  $\text{TbMnO}_3$ . The phason mode, which contributes little to the data in Fig. 5, must possess a much smaller energy at the magnetic zone center. Both modes visible in Fig. 5 exhibit larger widths than what can be explained by the resolution (FWHM  $\sim 0.2\text{ meV}$ ). This can be a consequence of the anharmonic folding discussed in reference<sup>38</sup>.

Due to the less favorable scattering conditions with the small sample only the dispersion along the  $b$  direction and the zone boundary along  $c$  could be studied. The scans taken at the latter positions,  $(0\ 0.363\ 1.5)$  and  $(0\ 0\ 1.5)$  indicate a double signal near 4 meV which again agrees with the dispersion reported for  $\text{TbMnO}_3$ . In this direction only the antiferromagnetic coupling along the  $c$  direction intervenes, which amounts to about  $J_{AFM} = -0.5\text{ meV}$  and which is little reduced between  $\text{LaMnO}_3$ <sup>52</sup> and  $\text{TbMnO}_3$ <sup>43,53</sup>, as well as between  $\text{TbMnO}_3$  and  $\text{DyMnO}_3$ .

The total dispersion along  $b$  ranging from  $\vec{Q}=(0\ 0\ 1)$  and the magnetic Bragg to the boundary at  $\vec{Q}=(0\ 1\ 1)$  is shown in Fig. 7. The upper panel displays the raw data and the lower part the dispersion of the maxima obtained by fitting gaussian intensity distributions. As for  $\text{TbMnO}_3$  a split dispersion consisting of at least two



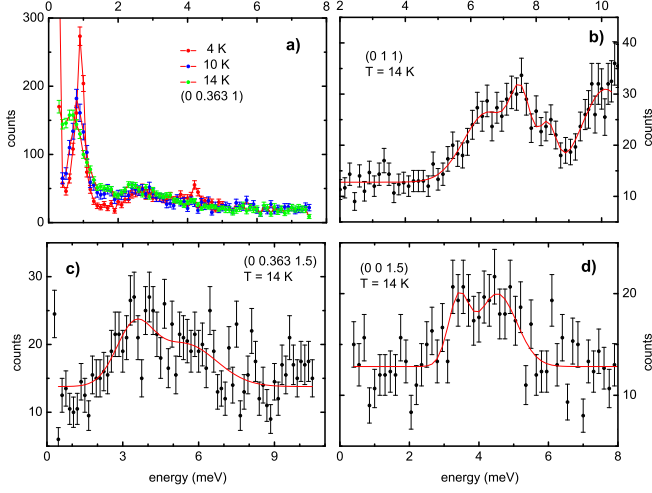


FIG. 6: (Color online) Constant  $\vec{Q}$  scans taken at various point in the Brillouin zone to establish the magnon dispersion in DyMnO<sub>3</sub>; a) magnetic zone center; b) end point of the dispersion in  $b$  direction; zone boundary in  $c$  direction with c) and without d) the incommensurate modulation along  $b$ .

or three branches can be followed across the entire zone reaching energies of 6 to 8 meV at the zone boundary, see Fig. 6b) where the signal at higher energy seems to arise from a phonon. This suggests that the ferromagnetic interaction between nearest neighbors in the  $ab$  planes,  $J_{FM}$ , is little renormalized when passing from the Tb to the Dy compound, in agreement with the small difference of the ionic radii<sup>43</sup>. The main difference in the magnon dispersion arises from the enhanced frustration by the next-nearest neighbor interaction along  $b$ ,  $J_{NNN} = -\eta \cdot J_{FM}$ , which results in a larger value of the incommensurate modulation vector in DyMnO<sub>3</sub>,  $q_k=0.36$  instead of 0.28 in TbMnO<sub>3</sub>. In DyMnO<sub>3</sub> the interaction ratio  $\eta$  amounts to 1.15 in comparison to the value of 0.78 in TbMnO<sub>3</sub>. This enhanced frustration is in full agreement with the stronger structural distortion arising from the slightly smaller ionic radius in DyMnO<sub>3</sub>. Further parameters needed to describe the dispersion are the antiferromagnetic exchange in  $c$  direction,  $J_{AFM}$ , the single-ion anisotropy term  $\Lambda$ , and the spin value  $S=2$  for Mn<sup>3+</sup>. The simple spin-only Hamiltonian of the magnetic interaction is given by:

$$\mathcal{H} = - \sum_{i,j} J_{i,j} \vec{S}_i \cdot \vec{S}_j - \Lambda \sum_i S_i^z, \quad (2)$$

where the sum only contains the nearest neighbors in the  $a, b$  planes,  $J_{FM}$ , nearest neighbors parallel to  $c$ ,  $J_{AFM}$ , and the next-nearest neighbors in the planes  $J_{NNN}$ . Besides for  $\eta$ , only slight modifications are needed to describe the magnon dispersion in TbMnO<sub>3</sub> and DyMnO<sub>3</sub>, see Fig. 7.

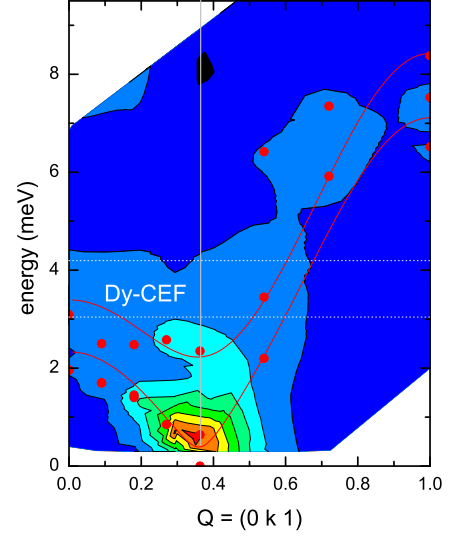


FIG. 7: (Color online) Dispersion of magnetic excitations along the  $b$  direction shown as a color contour plot of the scattered intensities. The lines denote the spin-wave dispersion calculated in linear theory as described in reference<sup>43</sup>. Parameters were  $J_{FM}=0.12(0.14)$ meV,  $J_{AFM}=-0.4(-0.35)$ meV and  $\Lambda=0.19(0.4)$ meV for the lower(upper) curves; red dots denote peak positions determined by fitting Gaussians to the measured scans.

Most interesting are the zone-center magnons as potential candidates for electromagnon modes. The temperature dependence of the two  $a$  polarized modes taken from the data in Fig. 6a) is shown in Fig. 8. Both modes harden upon cooling as expected. The energy of the lowest mode, which can be assigned to the CRM, perfectly agrees with the low-energy electromagnon signal detected recently in a THz radiation experiment<sup>5</sup>. As first proposed in reference<sup>14</sup> the rotation of the entire cycloid results in an electromagnon mode basing on the same magnetoelectric DM coupling as the static multiferroic phase, but the dielectric oscillator strength of this electromagnon mode is small.

The higher zone center mode near 2.5 meV, assigned to the HM, can be compared with electromagnon scattering observed in THz spectroscopy, see reference<sup>26</sup>. However, the largest peak in the THz radiation experiment (tracing  $\epsilon_2$ ) clearly exhibits a lower energy than the zone center magnon; for example at T=14 K the optical peak appears at  $\sim 1.7$  meV well below the magnon at 2.38(8) meV. The HM is not expected to exhibit strong polarization as the coupling between magnetic structure and polarization is quadratic. The intermediate-energy electromagnon scattering constitutes the strongest electromagnon signal in DyMnO<sub>3</sub> when tracing  $\epsilon_2$ <sup>26</sup>, but considering the oscillator strength both signals are comparable. In contrast, the high energy signal clearly dominates in TbMnO<sub>3</sub><sup>28</sup>. Another mechanism than the weak inverse DM interaction must be responsible for the intermediate optical sig-

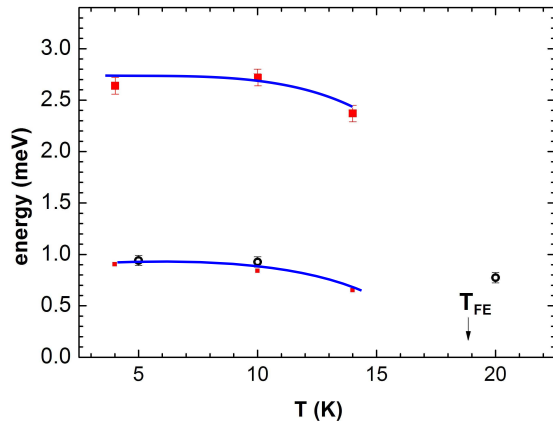


FIG. 8: (Color online) Temperature dependence of electro-magnons in DyMnO<sub>3</sub>: The inelastic neutron scattering results (filled black symbols) are compared with those of spectroscopic measurements<sup>5</sup> (open red symbols) for the lowest mode. Lines are guides to the eye.

nal. It has been proposed that the exchange striction mechanism combined with some backfolding of magnons is responsible for this strong low-energy scattering<sup>38</sup>. Indeed the branches connecting the magnetic zone center to  $\vec{Q}=(0\ 0\ 1)$  are quite flat, see Fig. 5b), giving support for such a picture; but this flat branch lies significantly above the energy of the THz radiation signal<sup>26</sup>.

In DyMnO<sub>3</sub>, the electromagnon signal found in the spectroscopic studies at highest energy appears at  $\sim 6$  meV at 14 K, but this signal only forms a shoulder in  $\epsilon_2$  for DyMnO<sub>3</sub>. Following the proposal of Valdés Aguilar et al. this electromagnon arises from the exchange striction mechanism and a magnetic arrangement that profits from an alternation of the magnetic exchange in  $b$  direction<sup>18</sup>. The static arrangement in a  $-\uparrow-\uparrow-\downarrow-\downarrow-$  structure (labelled E-type in  $REMO_3$  perovskites) couples to an alternation of enhancement and reduction of the ferromagnetic interaction in the bonds. This can be seen in the structure  $-\uparrow-J_{FM}^+-\uparrow-J_{FM}^--\downarrow-J_{FM}^--\downarrow-J_{FM}^+-\uparrow-$  where parallel moments profit from stronger ferromagnetic interaction. In a static cycloid with incommensurate modulation such an oscillating arrangement is not realized for the zone boundary magnon of the orthorhombic structure but for the magnon with a  $k$  component of the wave vector of  $k_{elm-str}=1-k_{inc}=0.637$ . This mode is illustrated in Fig. 1 d), which also indicates the variation of the scalar product of neighboring spin, which alternates. A magnon energy at this  $k$  value of the  $b$  dispersion indeed amounts to 6 meV in good agreement with the spectroscopic data, see Fig. 7. The fact that there is good agreement at quite different energies in DyMnO<sub>3</sub> and TbMnO<sub>3</sub> (for Tb this mode appears at 7.5 meV<sup>28,43</sup>) gives strong support for the exchange striction mechanism. The difference in the energies in DyMnO<sub>3</sub> and TbMnO<sub>3</sub> mainly

arises from the different incommensurate pitch with its impact on  $k_{elm-str}$ . It has been proposed that the strong low-energy peak in the optical response of DyMnO<sub>3</sub> and similar  $REMO_3$  compounds arises from strong backfolding of the magnon dispersion partially due to the local rotation of the magnetic anisotropy<sup>38</sup>. The measured dispersion, however, does not support fully such interpretation as the strong backfolding effects cannot be observed between  $(0\ 0.36\ 1)$  and  $(0\ 1\ 1)$  although the dispersion is flat between  $(0\ 0.36\ 1)$  and  $(0\ 0\ 1)$ , see Fig. 5 and 7. Further efforts are needed to fully understand the reasons of the strong electromagnon response slightly below the frequency of the HM.

#### IV. CONCLUSIONS

The study of the magnetic ordering confirms the close coupling between Mn and Dy moments which results in remarkable hysteresis effects. The intrinsic hysteresis of the Dy moment ordering together with the depinning of the incommensurate Mn modulation result in a complex hysteretic behavior which perfectly corresponds to the reported hysteresis in the temperature dependence of the ferroelectric and dielectric properties.

The comparison of the inelastic neutron scattering studies on the magnon dispersion in DyMnO<sub>3</sub> with previously reported spectroscopic measurements<sup>5,26</sup> helps identifying the electromagnon modes. The high-energy optical signal perfectly fits with the energy of the magnon mode that is expected to strongly couple via the exchange striction mode. Its energy is significantly lower than that of the corresponding mode in TbMnO<sub>3</sub> mainly due to the enhanced value of the incommensurate modulation. The zone-boundary magnon energies differ much less between DyMnO<sub>3</sub> and TbMnO<sub>3</sub> indicating similarly strong nearest-neighbor ferromagnetic interaction. Concerning the electromagnon excitation at the lowest energy, there is good agreement between the dielectric and our neutron scattering experiments. This mode can be identified as the cycloid rotation mode which gets its electromagnon weight by the same inverse Dzyaloshinski-Moriya mechanism as the static multiferroic order. Again this agrees with the observations for TbMnO<sub>3</sub><sup>43</sup>. Concerning the intermediate electromagnon signal, however, there is no agreement between the spectroscopic studies and the zone center magnons sensed by neutron scattering. This finding contrasts with the reports in TbMnO<sub>3</sub>. The strong spectral weight observed near 2 meV in the THz radiation studies must possess a different origin eventually related with back folding of magnon branches. Indeed the magnon dispersion seems to be quite flat between  $(0\ q_{inc}\ 1)$  and  $(0\ 0\ 1)$ .

*Acknowledgments.* This work was supported by the Deutsche Forschungsgemeinschaft through Sonderforschungsbereich 608 and contract AR 613/1-1.



- \* now at: European Spallation Source, S-22100 Lund, Sweden
- † Electronic address: braden@ph2.uni-koeln.de
- <sup>1</sup> G. A. Smolenskii and I. E. Chupis, Sov. Phys. Usp. **25**, 475 (1982).
  - <sup>2</sup> G. A. Smolenskii and I. E. Chupis, Sov. Phys. Usp. **25**, 475 (1983).
  - <sup>3</sup> I. Kézsmárki, N. Kida, H. Murakawa, S. Bordács, Y. Onose, and Y. Tokura, Phys. Rev. Lett. **106**, 057403 (2011).
  - <sup>4</sup> S. Bordács, I. Kézsmárki, D. Szaller, L. Demkó, N. Kida, H. Murakawa, Y. Onose, R. Shimano, T. Room, U. Nagel, S. Miyahara, N. Furukawa and Y. Tokura, Nat. Phys. **8**, 734 (2012).
  - <sup>5</sup> A. Shuvaev, V. Dziom, Anna Pimenov, M. Schiebl, A. A. Mukhin, A. C. Komarek, T. Finger, M. Braden, and A. Pimenov, Phys. Rev. Lett. **111**, 227201 (2013).
  - <sup>6</sup> Y. Yamasaki, S. Miyasaka, Y. Kaneko, J.-P. He, T. Arima, and Y. Tokura, Phys. Rev. Lett. **96**, 207204 (2006).
  - <sup>7</sup> T. Hoffmann, P. Thielen, P. Becker, L. Bohatý, and M. Fiebig, Phys. Rev. B **84**, 184404 (2011).
  - <sup>8</sup> M. Baum, J. Leist, Th. Finger, K. Schmalzl, A. Hiess, L. P. Regnault, P. Becker, L. Bohatý, G. Eckold, and M. Braden Phys. Rev. B **89**, 144406 (2014).
  - <sup>9</sup> T. Kimura, S. Ishihara, H. Shintani, T. Arima, K. Takahashi, K. Ishizaka, and Y. Tokura, Nature **426**, 55 (2003).
  - <sup>10</sup> T. Goto, T. Kimura, G. Lawes, A. Ramirez, and Y. Tokura, Phys. Rev. Lett. **92**, 257201 (2004).
  - <sup>11</sup> T. Kimura, G. Lawes, T. Goto, Y. Tokura, and A. Ramirez, Phys. Rev. B **71**, 224425 (2005).
  - <sup>12</sup> S.-W. Cheong and M. Mostovoy, Nature Mater. **6**, 13 (2007).
  - <sup>13</sup> A. Pimenov, A. Mukhin, V. Ivanov, V. Travkin, A. Balbashov, and A. Loidl, Nature Physics **2**, 97 (2006).
  - <sup>14</sup> H. Katsura, A. V. Balatsky, and N. Nagaosa, Phys. Rev. Lett. **98**, 027203 (2007).
  - <sup>15</sup> H. Katsura, N. Nagaosa, and A. Balatsky, Phys. Rev. Lett. **95**, 057205 (2005).
  - <sup>16</sup> M. Mostovoy, Phys. Rev. Lett. **96**, 067601 (2006).
  - <sup>17</sup> I. Sergienko and E. Dagotto, Phys. Rev. B **73**, 094434 (2005).
  - <sup>18</sup> R. Valdés Aguilar, M. Mostovoy, A. B. Sushkov, C. L. Zhang, Y. J. Choi, S.-W. Cheong, and H. D. Drew Phys. Rev. Lett. **102**, 047203 (2009).
  - <sup>19</sup> S. Quezel, F. Tcheou, J. Rossat-Mignod, G. Quezel, and E. Roudaut, **86-88**, 916 (1977).
  - <sup>20</sup> J. Blasco, C. Ritter, J. Garcia, J. de Teresa, J. Perez-Cacho, and M. Ibarra, Phys. Rev. B **62**, 5609 (2000).
  - <sup>21</sup> M. Kenzelmann, A. Harris, S. Jonas, C. Broholm, J. Schefer, S. Kim, C. Zhang, S.-W. Cheong, O. Vajk, and J. Lynn, Phys. Rev. Lett. **95**, 087206 (2005).
  - <sup>22</sup> R. Kajimoto, H. Yoshizawa, H. Shintani, T. Kimura, and Y. Tokura, Phys. Rev. B **70**, 012401 (2004).
  - <sup>23</sup> N. Aliouane, K. Schmalzl, D. Senff, A. Maljuk, K. Prokes, M. Braden, and D. N. Argyriou, Phys. Rev. Lett. **102**, 207205 (2009).
  - <sup>24</sup> R. Valdés Aguilar, A. B. Sushkov, C. L. Zhang, Y. J. Choi, S.-W. Cheong, and H. D. Drew Phys. Rev. B **76**, 060404(R) (2007).
  - <sup>25</sup> A. Pimenov, T. Rudolf, F. Mayr, A. Loidl, A. A. Mukhin, and A. M. Balbashov Phys. Rev. B **74**, 100403(R) (2006).
  - <sup>26</sup> N. Kida, Y. Ikebe, Y. Takahashi, J. P. He, Y. Kaneko, Y. Yamasaki, R. Shimano, T. Arima, N. Nagaosa, and Y. Tokura, Phys. Rev. B **78**, 104414 (2008).
  - <sup>27</sup> A. B. Sushkov, R. Valdés Aguilar, S. Park, S.-W. Cheong, and H. D. Drew, Phys. Rev. Lett. **98**, 027202 (2007).
  - <sup>28</sup> Y. Takahashi, N. Kida, Y. Yamasaki, J. Fujioka, T. Arima, R. Shimano, S. Miyahara, M. Mochizuki, N. Furukawa, and Y. Tokura, Phys. Rev. Lett. **101**, 187201 (2008).
  - <sup>29</sup> J. S. Lee, N. Kida, S. Miyahara, Y. Takahashi, Y. Yamasaki, R. Shimano, N. Furukawa, and Y. Tokura, Phys. Rev. B **79**, 180403 (2009).
  - <sup>30</sup> Y. Takahashi, Y. Yamasaki, N. Kida, Y. Kaneko, T. Arima, R. Shimano, and Y. Tokura Phys. Rev. B **79**, 214431 (2009).
  - <sup>31</sup> A. Pimenov, A. Shuvaev, A. Loidl, F. Schrettle, A. A. Mukhin, V. D. Travkin, V. Yu. Ivanov, and A. M. Balbashov, Phys. Rev. Lett. **102**, 107203 (2009).
  - <sup>32</sup> Y. Takahashi, Sh. Ishiwata, Sh. Miyahara, Y. Kaneko, N. Furukawa, Y. Taguchi, R. Shimano, and Y. Tokura Phys. Rev. B **81**, 100413(R) (2010).
  - <sup>33</sup> A. M. Shuvaev, V. D. Travkin, V. Y. Ivanov, A. A. Mukhin, and A. Pimenov, Phys. Rev. Lett. **104**, 097202 (2010).
  - <sup>34</sup> P. Rovillain, M. Cazayous, Y. Gallais, A. Sacuto, M.-A. Measson, and H. Sakata, Phys. Rev. B **81**, 054428 (2010).
  - <sup>35</sup> Y. Takahashi, R. Shimano, Y. Kaneko, H. Murakawa, and Y. Tokura, Nature Phys. **8**, 121 (2012).
  - <sup>36</sup> Y. Takahashi, Y. Yamasaki, and Y. Tokura, Phys. Rev. Lett. **111**, 037204 (2013).
  - <sup>37</sup> A. Cano, Phys. Rev. B **80**, 180416(R) (2009).
  - <sup>38</sup> M. Mochizuki, N. Furukawa, and N. Nagaosa, Phys. Rev. Lett. **104**, 177206 (2010).
  - <sup>39</sup> M.P.V. Sternberg and R. de Soussa, Phys. Rev. B **80**, 094419 (2009).
  - <sup>40</sup> M.P.V. Sternberg and R. Soussa, Phys. Rev. B **85**, 104412 (2012).
  - <sup>41</sup> T. Hasegawa, S. Miyahara and N. Furukawa, J. Phys.: Conf. Ser. **200**, 012053 (2010).
  - <sup>42</sup> D. Senff, P. Link, K. Hradil, A. Hiess, L. P. Regnault, Y. Sidis, N. Aliouane, D. N. Argyriou, and M. Braden, Phys. Rev. Lett. **98**, 137206 (2007).
  - <sup>43</sup> D. Senff, N. Aliouane, D. N. Argyriou, A. Hiess, L. P. Regnault, P. Link, K. Hradil, Y. Sidis, and M. Braden, J. Phys. Condens. Matter **20**, 434212 (2008).
  - <sup>44</sup> D. Senff, P. Link, N. Aliouane, D. N. Argyriou, and M. Braden Phys. Rev. B **77**, 174419 (2008).
  - <sup>45</sup> R. Feyerherm, E. Dudzik, N. Aliouane, and D. N. Argyriou Phys. Rev. B **73**, 180401(R) (2006).
  - <sup>46</sup> O. Prokhnenko, R. Feyerherm, E. Dudzik, S. Landsgesell, N. Aliouane, L. C. Chapon, and D. N. Argyriou Phys. Rev. Lett. **98**, 057206 (2007).
  - <sup>47</sup> J. Strempfer, B. Bohnenbuck, M. Mostovoy, N. Aliouane, D. N. Argyriou, F. Schrettle, J. Hemberger, A. Krimmel, and M. v. Zimmermann Phys. Rev. B **75**, 212402 (2007).
  - <sup>48</sup> T. Cronert, diploma thesis, University of Cologne (2014).
  - <sup>49</sup> Ch. Lu, S. Dong, Z. Xia, H. Luo, H. Wang, Z. Tian, S. Yuan, T. Wu, and J. Liu, Sci. Rep. **3**, 3374; DOI:10.1038/srep03374 (2013).
  - <sup>50</sup> S. Jandl, S. Mansouri, A. A. Mukhin, V. Yu. Balbashov, and M. M. Gospodino, J. of Magn. and Magn. Materials **323**, 1104 (2011).
  - <sup>51</sup> Marshall W and Lovesey S W 1971 *Theory of Thermal*

- Neutron Scattering* (Oxford : Clarendon Press)
- <sup>52</sup> F. Moussa, M. Hennion, J. Rodríguez-Carvajal, H. Moudén, L. Pinsard, and A. Revcolevschi, Phys. Rev. B **54** 15149 (1996).
- <sup>53</sup> R. Kajimoto, H. Mochizuki, H. Yoshizawa, H. Shintani, T. Kimura, and Y. and Tokura, J. Phys. Soc. Japan **74**, 2430 (2005).